Acta Oceanol. Sin., 2024, Vol. 43, No. 5, P. 100–109
https://doi.org/10.1007/s13131-024-2322-y
http://www.aosocean.com
E-mail: ocean2@hyxb.org.cn

An improved wind quality control for the China-France Oceanography Satellite (CFOSAT) scatterometer

Xiaoheng Mou[1], Wenming Lin[1, 2*]

[1] School of Marine Sciences, Nanjing University of Information Science and Technology, Nanjing 210044, China

[2] Key Laboratory of Space Ocean Remote Sensing and Application, Ministry of Natural Resources, Beijing 100081, China

Received 26 December 2023; accepted 28 February 2024

Abstract

Quality control (QC) is an essential procedure in scatterometer wind retrieval, which is used to distinguish good-quality data from poor-quality wind vector cells (WVCs) for the sake of wind applications. The current wind processor of the China-France Oceanography Satellite (CFOSAT) scatterometer (CSCAT) adopts a maximum likelihood estimator (MLE)-based QC method to filter WVCs affected by geophysical noise, such as rainfall and wind variability. As the first Ku-band rotating fan-beam scatterometer, CSCAT can acquire up to 16 observations over a single WVC, giving abundant information with diverse incidence/azimuth angles, as such its MLE statistical characteristics may be different from the previous scatterometers. In this study, several QC indicators, including MLE, its spatially averaged value (MLE_m), and the singularity exponents (SE), are analyzed using the collocated Global Precipitation Mission rainfall data as well as buoy data, to compare their sensitivity to rainfall and wind quality. The results show that wind error characteristics of CSCAT under different QC methods are similar to those of other Ku-band scatterometers, i.e., SE is more suitable than other parameters for the wind QC at outer-swath and nadir regions, while MLE_m is the best QC indicator for the sweet region WVCs. Specifically, SE is much more favorable than others at high wind speeds. By combining different indicators, an improved QC method is developed for CSCAT. The validation with the collocated buoy data shows that it accepts more WVCs, and in turn, improves the quality control of CSCAT wind data.

Key words: China-France Oceanography Satellite (CFOSAT), scatterometer, winds, quality control (QC), singularity exponent (SE)

Citation: Mou Xiaoheng, Lin Wenming. 2024. An improved wind quality control for the China-France Oceanography Satellite (CFOSAT) scatterometer. Acta Oceanologica Sinica, 43(5): 100–109, doi: 10.1007/s13131-024-2322-y

1 Introduction

Spaceborne microwave scatterometers are widely used to observe global sea surface backscatter coefficients in relatively high spatial and temporal resolutions, and in turn, are the primary technique for acquiring the mesoscale sea surface winds (Pierson, 1989; Stoffelen and Anderson, 1997). To date, the China-France Oceanography Satellite (CFOSAT) scatterometer (CSCAT) together with other in-orbit scatterometers have consisted of a virtual wind observation constellation that helps to improve the accuracy of wind measurements and to realize high-frequency acquisitions of global ocean wind vectors (Portabella et al., 2021). Although the antenna of CSCAT stopped spinning in December 2022, it still provides valuable data for the study of Ku-band sea surface backscattering characteristics, since the fanbeam antenna covers a wide incidence range from 28° to 51° (Lin et al., 2019; Liu et al., 2020). Therefore, CSCAT data reprocessing has recently been initiated with the aim of providing temporally consistent and high-quality winds information (Mou et al., 2023; Mironov et al., 2023).

In practice, however, there are many non-wind geophysical phenomena that may enhance or attenuate the sea surface backscattering signal during the scatterometer measurement procedure, such as rainfall, wind variability, confused sea states, and other oceanic/atmospheric processes (Portabella and Stoffelen, 2002a; Stiles and Dunbar, 2010; Portabella et al., 2012; Lin et al., 2015b). Among the above, rain is the main factor in degrading the retrieved wind quality of scatterometers. In general, C-band scatterometers have longer wavelengths than Ku-band ones, such that their wind quality is more stable than the latter in the presence of rain (Stiles and Yueh, 2002; Tournadre and Quilfen, 2003; Weissman and Bourassa, 2008; Lin et al., 2015a). In other words, the quality control (QC) module for the Ku-band scatterometer wind inversion process is very critical, which can not only help to reject poor quality scatterometer wind vector cells (WVCs) but also impact on the application of the scatterometer winds, such as data assimilation in numerical weather prediction (NWP) model, typhoon monitoring and other aspects of weather forecasting (Brennan et al., 2009; Xu et al., 2019; Liu et al., 2022; Chen et al., 2023). Similar to the Pencil-Beam Wind Processor (PenWP) provided by the Ocean and Sea Ice Satellite Application Facility (OSI SAF) of the European Organization for the Exploitation of Meteorological Satellites (EUMETSAT) (Verhoef et al., 2015), the current CSCAT wind processor uses the inversion residuals as an indicator of the wind quality, which rep-

Foundation item: The National Key Research and Development Program of China under contract Nos 2022YFC3104900 and 2022YFC3104902.

*Corresponding author, E-mail: wenminglin@nuist.edu.cn

resents the distance between the measured backscatters and the simulated ones from the wind geophysical model function (GMF). Conventionally, the maximum likelihood estimator is used to perform wind inversion for the scatterometers, hence the inversion residuals are usually named as MLE (Stoffelen and Portabella, 2006). Basically, large MLE values correspond to poor-quality wind retrievals, and vice versa. It is important to note that different scatterometers require instrument-specific QC thresholds to accept wind cells with good quality. The overall WVC rejection rate is normally around 6% for the Ku-band scatterometers, although it can be as much as 20% at high wind speeds and roughly 1% at low wind (Lin and Portabella, 2017).

Numerous quality indicators and techniques have been put forth to date with the aim of improving scatterometer quality control and minimizing the rejection of valuable WVCs. For instance, the singularity exponent (SE) derived from the singularity analysis (SA) image processing technique, has been demonstrated to be useful for Advanced Scatterometer (ASCAT) and RapidScat (RSCAT) QC, due to its capability in identifying rainfall and wind variability within the wind cell, especially for the low winds of the ASCAT and the outer swath of the RSCAT (Lin et al., 2014, 2016; Lin and Portabella, 2017). In addition, since the maximum likelihood estimator (MLE) has been proven to have good performance in the scatterometer QC process (Portabella and Stoffelen, 2001, 2002b), the spatially-averaged MLE (MLE_m) was proposed to further improve the scatterometer wind QC by taking into account the spatial gradient characteristics of the WVCs, which latter has been applied to the wind QC for the inner swath of the RSCAT and the high speeds of the HY-2 scatterometers (HSCAT) (Lin and Portabella, 2017; Lang et al., 2022). In order to improve rain screening for the Ku-band scatterometers, a QC indicator (namely J_{OSS}) derived from the two-dimensional variational ambiguity removal (2DVAR) procedure of the wind retrieval has been proposed, which has apparently reduced the rain false alarm rate for both CSCATA and the Scatterometer onboard the Scatsat-1 Satellite (OSCAT-2) (Xu and Stoffelen, 2020; Xu et al., 2022). Last but not least, there are also many other rainfall identification algorithms, such as the multi-dimensional histogram rain-flagging technique (MUDH) and the K-Nearest Neighborhood (KNN) method (Huddleston and Stiles, 2000; Peng et al., 2021).

The aim of this paper is to find good quality indicators for the CSCAT wind QC, since the CSCAT inversion residuals may have different characteristics from the previous scatterometers, due to its innovative observation geometry. Section 2 describes the CSCAT data, buoy data, and rainfall data used in this study. The calculation of the quality indicators is also briefly summarized. Section 3 analyzes the quality of the wind field with different indicators. In Section 4, their rain detection features are analyzed, and then a novel quality control approach using a simple combination of those indicators is proposed for CSCAT. Finally, the conclusions are presented in Section 5.

2 Data and method

2.1 *Wind and precipitation data*

The reprocessed wind product for the entire year of 2021 is used to evaluate the capacity of different quality indicators in terms of identifying low-quality wind vector cells. Note that the reprocessed scatterometer wind product is obtained by applying the weekly NWP ocean calibration (NOC) coefficients to the winds inversion, which requires the level 1B data supplied by the National Satellite Ocean Application Service (NSOAS) as the input. For the purpose of analyzing the CSCAT wind differences under various quality control methods, the European Centre for Medium-Range Weather Forecasts (ECMWF) winds are used as the reference because of their numerous collocations and consistent wind quality (Zhao et al., 2022). By using temporal and spatial interpolation on three 3-hourly ECMWF forecast winds, the ECMWF background winds are then included in the Level 2 product of the CSCAT reprocessed winds. Figure 1 illustrates the relationship between the wind speed bias and the sorted MLE value, where the MLE are ranked according to their values from largest to smallest. The results show that the reprocessed data is more consistent with the MLE-based QC threshold (black dashed curve) than that of the operational near-real-time (NRT) product (Fig. 1a), which verifies that the reprocessed CSCAT winds are of better quality than the NRT data.

Furthermore, the moored buoy winds (January–December 2021) are collocated with CSCAT data in order to validate the ef-

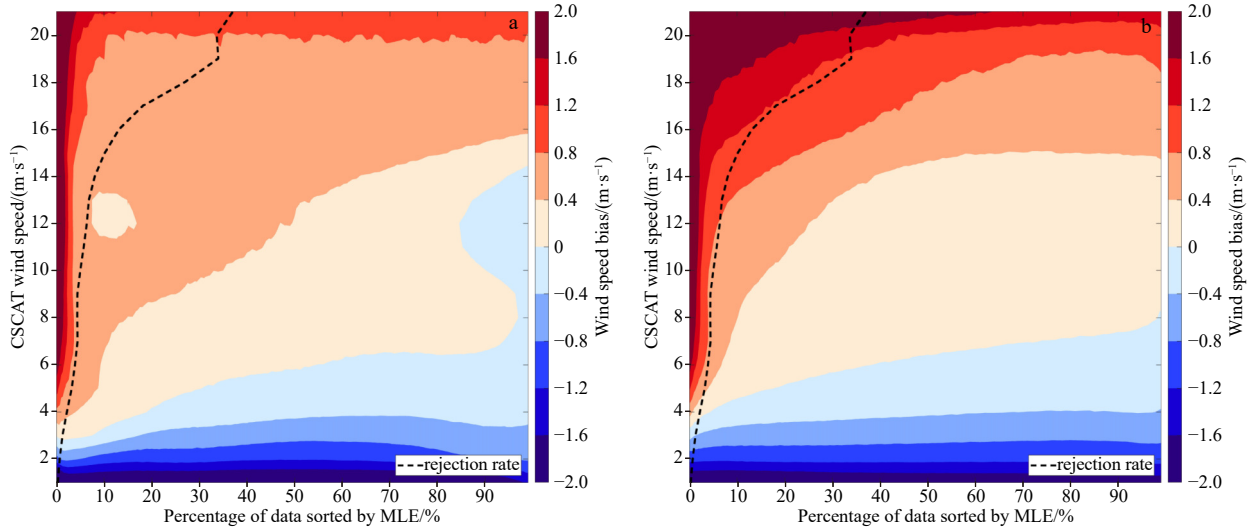

Fig. 1. Wind speed bias as a function China-France Oceanography Satellite scatterometer (CSCAT) wind speed and the sorted percentiles by maximum likelihood estimator (MLE) for the near-real-time wind product (a) and the reprocessed wind data (b). The black dashed curve indicates the rejection ratio of the operational MLE-based quality control.

fectiveness of the quality control methodology applied to the reprocessed winds. To make buoy winds comparable to the CSCAT winds, the Liu-Katsaros-Businger (LKB) model is utilized to convert buoy data into 10-m equivalent-neutral winds (Liu et al., 1979). The principle of obtaining the collocation is that the buoy winds are less than 25 km and 30 min distance from the CSCAT acquisitions. Finally, the total amount of CSCAT–buoy collocations is about 90.7 k.

As the successor of the Tropical Rainfall Measuring Mission (TRMM), the Global Precipitation Measurement (GPM) mission has realized high-frequency observations of rainfall in most regions of the world (Prakash et al., 2016). The rain rate (RR) used here is from Integrated Multi-satelliE Retrievals for GPM (IMERG) product, with at least ten passive and active instruments data involved in it (Huffman et al., 2018). As the level 3 product, it offers three different products (i.e., Early, Late, and Final) for users, among which the Final one can reach research quality. This study employs the latest (version 7) half-hourly Final rainfall data with a spatial resolution of 0.1° to assess the CSCAT wind quality under rainy conditions. The collocation criteria for IMERG are the same as above. In case that there is more than one IMERG rain value collocated with CSCAT, the one with the closest spatial distance to the CSCAT position is selected. Eventually, the amount of IMERG-CSCAT collocations is about 187 million. This dataset can be used to assess the sensitivity of different quality indicators to rainfall.

2.2 *QC indicators*

Wind inversion residual (i.e., MLE) is acquired during the scatterometer wind inversion process, which value reflects directly the quality of the wind, hence it is commonly used as an indicator for quality control. The MLE is calculated as follows:

$$\mathrm{MLE} = \frac{1}{N}\sum_{i=1}^{N}\frac{(\sigma^0_{\mathrm{m}i} - \sigma^0_{\mathrm{s}i})^2}{(K_{\mathrm{p}i}\sigma^0_{\mathrm{m}i})^2}, \tag{1}$$

where N is the number of observations within a wind vector cell, $\sigma^0_{\mathrm{m}i}$ is the measured backscatter coefficient of the i-th observation, $K_{\mathrm{p}i}$ is the normalized measurement error, and σ^0_{si} represents the simulated backscatter coefficient, which is obtained from the background wind information and the NSCAT-4 GMF. Therefore, the MLE value represents the distance between the measured σ^0_{s} and the simulated backscatter values. A large MLE value denotes that the difference between the above two is significant, indicating the low quality of the scatterometer-derived wind. In practice, a WVC is flagged as a rain-contaminated result or poor-quality retrieval if the corresponding MLE value exceeds a certain threshold, which is related to the scatterometer wind speed and the WVC number. As such, MLE is selected as a quality control indicator in CSCAT NRT products.

In order to better identify the WVCs affected by large inter- and/or sub-WVC wind variability, which is often found in areas of intensive convection, a spatially averaged MLE method (i.e., $\mathrm{MLE_m}$) is proposed to further improve the wind QC. $\mathrm{MLE_m}$ is derived from a centered 3 × 3 box (3 × 2 box used when WVCs are located at swath edge) and it can be simply calculated by the following formula:

$$\mathrm{MLE_m} = \frac{\sum_i w_i \mathrm{MLE}_i}{\sum_i w_i}, \tag{2}$$

where w_i is the weighting coefficient for the i-th WVC, which value is 4 for the centered WVC, 3 for the four WVCs adjoining to the center, and 2 for the rest positions.

Another QC indicator named SE is proposed to evaluate the spatial continuity and improve the quality control of the scatterometer winds. SE is derived from the following singularity analysis:

$$\mathrm{SE}(x) = \frac{\log_2[T_\psi \|\nabla s\|\,(x,r)/\langle T_\psi \|\nabla s\|\,(\cdot,r)\rangle]}{\log_2 r_0} + o\left(\frac{1}{\log_2 r_0}\right), \tag{3}$$

where $T_\psi||\nabla s||\,(x,r)$ is the wavelet projection of the objective signal s at the location x in the scale factor r, $\langle T_\psi||\nabla s||\,(\cdot,r)\rangle$ is the mean value of the wavelet projection over the whole signal, and $||\nabla s||$ represents the vector norm of the gradient of the signal. Specially, $T_\psi||\nabla s||$ is derived from the wind speed zonal (u) and meridional (v) components, as well as the MLE field. The scale r_0 is defined as the smallest accessible scale, while the mathematical symbol o stands for the infinitesimal of higher order. In this study, the SE data are directly acquired from the level 2 product of CSCAT.

3 Analysis of quality indicators

3.1 *Comparison with NWP winds*

It is well known that the wind quality of the Ku-band scatterometer is mainly affected by rainfall. Moreover, the percentage of rain-contaminated CSCAT data, as well as the rain rate, usually increases with the wind speed. Therefore the two collocations consisting of NWP and buoy data are firstly separated into low wind speeds ($w \leqslant 2$ m/s), medium wind speeds (2 m/s < $w \leqslant 14$ m/s), and high wind speeds ($w > 14$ m/s), respectively. In addition, as aforementioned, the MLE QC threshold is related to the WVC position, which has already been verified for CSCAT, and shows that the wind speed bias is connected to the scatterometer cross-track position and the magnitude of the rain rate. Hence, the collocations are further divided into several categories according to the WVC number, i.e., the outer swath (WVC numbers 1–5 and 38–42), the sweet swath (WVC numbers 6–17 and 26–37) and the nadir swath (WVC numbers 18–25). WVCs at the outer swath and the nadir region are observed with poor azimuth diversity, such that their wind quality is inherently poorer than the WVCs at the sweet swath, which latter are actually with redundant observation geometries (Liu et al., 2020). Figure 2 shows the three swaths associated with the CSCAT along-track data, in which the WVCs are numbered from the left-most WVC to the right-most one in ascending order. In order to guarantee that the analysis of wind differences is unaffected by data volume, the QC thresholds for MLE, $\mathrm{MLE_m}$, and SE are adapted to achieve the same rejection rate as a function of wind speed.

Scatterometer wind quality is usually evaluated using the vector root mean square (VRMS) score, which is a reliable indicator by combining the differences in both wind speed and direction. The VRMS value is calculated as follows:

$$\mathrm{VRMS} = \sqrt{\frac{1}{N}\sum_{i=1}^{N}[(u_i^{\mathrm{scat}} - u_i^{\mathrm{ref}})^2 + (v_i^{\mathrm{scat}} - v_i^{\mathrm{ref}})^2]}, \tag{4}$$

where (u_i^{scat}, v_i^{scat}) and (u_i^{ref}, v_i^{ref}) are the i-th scatterometer and reference wind vectors, respectively; and N is the number of collocations. The NWP winds usually serve as the background winds in scatterometer wind retrieval, which could be a good reference

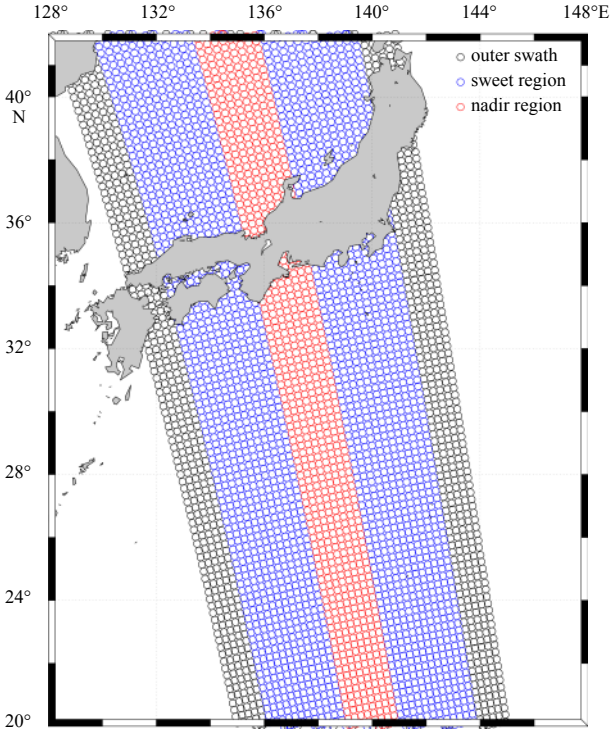

Fig. 2. Illustration of the wind vector cells at different swaths. Black, blue, and red circles represent the outer swath, the sweet region, and the nadir region, respectively.

in most conditions, such that the wind difference between scatterometer and NWP background winds is often used to assess the scatterometer-derived wind quality. Figure 3 shows the VRMS difference between CSCAT and NWP, and the percentage of rain-contaminated data with GPM rain rate larger than 0 mm/h, as a function of the sorted percentiles by MLE (blue line), MLE_m (red line), and SE (yellow line), respectively. Again, it shows that CSCAT wind quality is highly correlated with rainfall, i.e., the VRMS scores increase as the percentage of rain-contaminated WVCs increases. However, in the inner swath, MLE_m is excellent in identifying rainfall, but it does not detect as many low-quality WVCs as SE. On the other hand, SE is better than the other two indicators in distinguishing wind cells with large differences between CSCAT and NWP, though it is poorer than the other two indicators in terms of identifying rainfall. This may be due to the characteristics of CSCAT observation geometry, indicating that the scatterometer wind inversion with multiple incidence/azimuth angles may lead to a wind quality more tolerable to rainfall, even though the radar works at Ku-band. Moreover, it also means that CSCAT is more sensitive to other geophysical factors. In addition, the signal-to-noise ratio of the radar is essential for obtaining accurate sea surface backscatter coefficients, which directly affects the quality of the wind vector, thus causing the variability of data quality at different swaths of the CSCAT.

Table 1 shows the VRMS difference between CSCAT and NWP winds after applying the three QC indicators under different wind situations. Since NWP does not well resolve sea surface wind variability at low wind speeds, it can be found that at wind speeds less than 2 m/s, the VRMS scores of the accepted WVCs are close

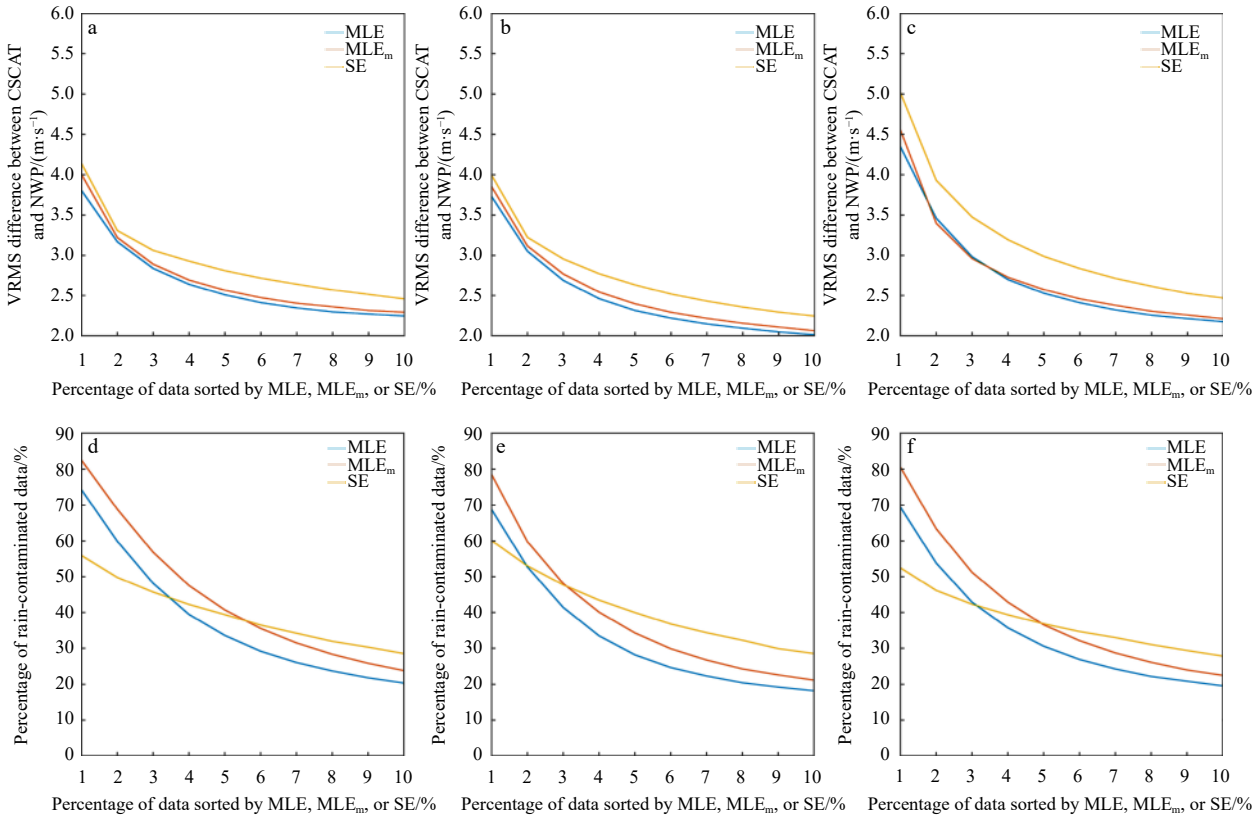

Fig. 3. VRMS difference between China-France Oceanography Satellite scatterometer (CSCAT) and numerical weather prediction (NWP) (upper panels), and the percentage of rain-contaminated data (GPM RR > 0 mm/h) (lower panels), as a function of the sorted percentiles by maximum likelihood estimator (MLE, blue), averagred MLE (MLE_m, red), and singularity exponents (SE, yellow) for the nadir region (a and d), the sweet region (b and e), and the outer swath (c and f), respectively.

Table 1. VRMS difference between China-France Oceanography Satellite scatterometer and numerical weather prediction winds categorized by different quality control (QC) methods under different wind speed conditions

Wind speed/(m·s^{-1})	Statistical results over the QC accepted data/(m·s^{-1})			Statistical results over the QC rejected data/(m·s^{-1})		
	MLE	MLE_m	SE	MLE	MLE_m	SE
$w \leqslant 2$	1.96	1.96	1.96	2.24	2.22	2.28
$2 < w \leqslant 14$	1.92	1.91	1.90	3.54	3.60	3.74
$w > 14$	2.16	2.14	2.08	2.88	2.95	3.19

to the rejected ones for any QC indicator, such that it is difficult to determine which indicator is more reliable for wind QC. Additionally, the three metrics are relatively comparable in terms of retaining high-quality winds at moderate wind speeds. The sensitivity of SE to data quality is better than that of the others under high wind conditions, whereas the statistics of MLE_m and MLE are relatively close to each other. In summary, the three QC indicators show distinct differences in both flagging rain and identifying poor-quality winds with respect to the NWP winds. MLE_m is generally optimal for the rain-flagging purpose, while SE is the best indicator in filtering the WVCs with high wind variability because it is derived from the local wind gradient.

3.2 *Comparison with buoy winds*

To mitigate potential wind errors introduced by the reference NWP winds, the QC indicators are further verified using the collocated CSCAT-buoy dataset in this study. Compared to the CSCAT-NWP collocations, the amount of buoy dataset is relatively limited, hence it is not feasible to derive the QC thresholds from the CSCAT-buoy dataset. Consequently, the QC thresholds are established based on the collocations with NWP winds and then are applied to filter WVCs in the CSCAT-buoy collocations. The VRMS difference between CSCAT and buoy winds, categorized by different indicators across various wind speed bins, are presented in Table 2. Notably, at lower and moderate wind speeds, the quality of accepted WVCs exhibits similarities, while the SE is able to identify a larger number of WVCs with poorer quality compared to the other indicators. Moreover, under high wind conditions, SE shows the highest sensitivity to wind quality, which effectively discriminates low-quality WVCs from good-quality ones.

The QC performance of the above three indicators over different swath regions is further examined in Table 3. Compared to SE, MLE_m and MLE are generally both with less efficacy in discerning between good- and poor-quality WVCs over the entire swaths. This is in line with the results of Section 3.1. More interestingly, the VRMS score of the MLE_m-rejected WVCs is larger than that of the other two indicators at the sweet swath, while the MLE_m-accepted WVCs are of poorer quality than SE-accepted ones. This is probably due to that the MLE_m detects more rain than SE at the sweet swath. Nonetheless, MLE_m is generally better than MLE for the wind QC purpose, similar to the previous studies on the other Ku-band scatterometers (Lang et al., 2022; Lin and Portabella, 2017).

4 Discussions

4.1 *CSCAT-GPM Analysis*

Since rainfall is the primary factor influencing the quality of Ku-band scatterometer winds, the effectiveness of quality indicators in identifying rainy WVCs is often employed as an additional evaluation approach. Figure 4 illustrates the percentage of rain-contaminated measurements (with rain rate above 1 mm/h) as a function of scatterometer-derived wind speed and the sorted percentiles by the three quality indicators. The rejection rate of WVCs as a function of wind speed is depicted by the black dashed line in the plots, which is the same for all three QC indicators. It is noteworthy that MLE and MLE_m are sorted in descending order, while SE is sorted in ascending order, such that the left side of x-axes always indicate poor-quality wind measurements. The objective rejection rate (black dashed curve) aligns well with the contour lines at moderate wind speeds. While at high wind speeds, the objective rejection rate does not show good agreement with the rain contour lines. Regarding that the main purpose of this paper is to find a suitable method for the CSCAT wind QC rather than for the rain detection, the objective rejection rate is not adapted to align with the rain contours under high wind conditions in this section. Nonetheless, MLE and MLE_m demonstrate good sensitivity to rainfall, such that they are able to filter a higher percentage of rain-contaminated data than SE. The area of rainy bins in Fig. 4c is significantly larger than that of the other two indicators, which is in line with the results of Fig. 3.

Table 2. VRMS difference between China-France Oceanography Satellite scatterometer and buoy winds categorized by different quality control (QC) methods in different wind speed bins

Wind speed/(m·s^{-1})	Statistical results over the QC accepted data/(m·s^{-1})			Statistical results over the QC rejected data/(m·s^{-1})		
	MLE	MLE_m	SE	MLE	MLE_m	SE
$w \leqslant 2$	2.26	2.25	2.23	4.84	4.54	5.71
$2 < w \leqslant 14$	2.56	2.54	2.50	5.49	5.47	5.92
$w > 14$	5.37	4.87	4.64	6.51	7.40	7.62

Table 3. VRMS difference between China-France Oceanography Satellite scatterometer and buoy winds categorized by different quality control (QC) methods for WVCs at different swath

Swath	Statistical results over the QC accepted data/(m·s^{-1})			Statistical results over the QC rejected data/(m·s^{-1})		
	MLE	MLE_m	SE	MLE	MLE_m	SE
Nadir region	2.81	2.87	2.71	4.72	5.31	5.83
Sweet region	2.62	2.73	2.56	5.41	5.85	5.73
Outer swath	2.98	3.11	2.88	5.81	5.79	6.19

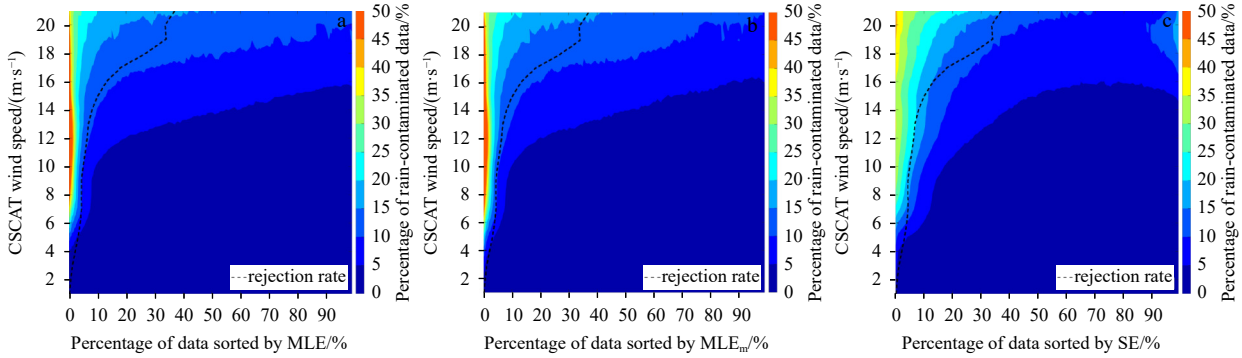

Fig. 4. Percentage of rain-contaminated data (GPM RR > 1 mm/h) as a function CSCAT wind speed and the sorted percentiles by maximum likelihood estimator (MLE, a), averaged MLE (MLE$_m$, b), and singularity exponents (SE, c). The black dashed curve indicates the (objective) rejection ratio of the operational MLE-based quality control.

Table 4 presents the percentage of rainy WVCs in the rejected data for the three indicators at various WVC positions, including statistical scores for rain rates above 0 mm/h and 1 mm/h. Notably, MLE$_m$ demonstrates the best capability to monitor rainy wind cells over the entire observation swaths, particularly in the sweet region. Since MLE$_m$ also rejects the worst quality WVCs w.r.t. buoy winds at the sweet swath, it can be concluded that the MLE$_m$ QC is more robust than SE and MLE at this specific location. Note also that the values in Table 4 are smaller than those of pencil-beam scatterometers (Lang et al., 2022), indicating that CSCAT is less sensitive to rainfall compared to other Ku-band scatterometers, probably due to its innovative observation mechanism. Overall, SE and MLE$_m$ both improve the CSCAT wind QC compared to the operational MLE-based QC, and MLE$_m$ can be also used to identify a larger amount of rainfall at the sweet swath.

Table 5 further evaluates the sensitivity of the three QC indicators to rainfall under different wind speed conditions. The analysis reveals that SE can identify more rain data than MLE and MLE$_m$ at both low and high wind speeds, whereas MLE$_m$ detects the most amount of rain-contaminated data at moderate wind speeds. This is due to that the rain-induced wind variability is most likely to associate with low and high wind conditions as a result, SE tends to detect more rainfall than the other indicators by actually identifying more variable sea surface winds. Tables 6 and 7 show the percentages of rain-contaminated data at different swaths and wind speed bins, respectively. The results are consistent with the above analysis, and it is noteworthy that all QC techniques detect a lower proportion of rainy data than the previous pencil-beam scatterometers. This implies that rainfall might not have as much impact on the CSCAT as the pencil-beam scatterometers (Zhao et al., 2022).

4.2 *Typhoon case study*

To visualize the QC effects, Fig. 5 depicts a scenario of Super Typhoon Mindulle, together with several QC indicators at high wind speeds. Here black arrows represent QC-accepted wind vectors, while white arrows represent QC-rejected ones. The pixel color corresponds to CSCAT wind speed, forming a comprehensive comparison under different wind speed conditions. It is

Table 4. Percentage of rain contaminated data (with GPM RR > 0 mm/h or GPM RR >1 mm/h) for the quality control (QC)-rejected data by different quality indicators over the three swath regions

Swath	Percentage of GPM RR > 0 mm/h over the QC rejected data/%			Percentage of GPM RR > 1 mm/h over the QC rejected data/%		
	MLE	MLE$_m$	SE	MLE	MLE$_m$	SE
Nadir region	51.0	58.5	47.7	24.1	28.1	20.0
Sweet region	54.3	61.3	50.4	26.1	29.8	22.4
Outer swath	48.9	55.2	53.0	23.4	26.8	25.0

Table 5. Percentage of rain contaminated data (with GPM RR > 0 mm/h or GPM RR >1 mm/h) over the quality control (QC)-rejected data by different QC indicators in different wind speed bins

Wind speed/ (m·s^{-1})	Percentage of GPM RR > 0 mm/h over the QC rejected data/%			Percentage of GPM RR > 1 mm/h over the QC rejected data/%		
	MLE	MLE$_m$	SE	MLE	MLE$_m$	SE
$w \leqslant 2$	8.5	23.3	31.5	1.2	4.7	5.8
$2 < w \leqslant 14$	54.5	61.0	50.1	28.1	31.4	23.7
$w > 14$	52.3	53.3	57.7	17.7	18.7	21.1

Table 6. Percentage of rain-contaminated data (with GPM RR > 0 mm/h or GPM RR > 1 mm/h) over the quality control-rejected WVCs for different swaths

Swath	Percentage of GPM RR > 0 mm/h over all rain contaminated data/%			Percentage of GPM RR > 1 mm/h over all rain contaminated data/%		
	MLE	MLE$_m$	SE	MLE	MLE$_m$	SE
Nadir region	17.1	19.0	16.1	8.1	9.1	6.7
Sweet region	18.6	20.3	17.3	8.9	9.9	7.7
Outer swath	16.8	18.3	18.2	8.0	8.9	8.6

Table 7. Percentage of rain contaminated data (with GPM RR > 0 mm/h or GPM RR > 1 mm/h) over the quality control-rejected wind vector cells for different wind speed bins

Wind speed/(m·s^{-1})	Percentage of GPM RR > 0 mm/h over all rain contaminated data/%			Percentage of GPM RR > 1 mm/h over all rain contaminated data/%		
	MLE	MLE_m	SE	MLE	MLE_m	SE
$w \leqslant 2$	1.6	3.9	6.1	0.2	0.8	1.2
$2 < w \leqslant 14$	17.7	19.9	16.6	9.1	10.2	7.8
$w > 14$	19.1	19.0	20.7	6.5	6.7	7.5

observed that spiral rainbands often accompany the typhoon. In case of high winds, both MLE and MLE_m retain most of the WVCs, whereas SE rejects a significant portion of data, most of which are indeed with rainfall. Compared to the rain rate image (Fig. 5d), the SE-rejected data also has more detailed features than those rejected by MLE and MLE_m. However, this also results in an exclusion of a considerable amount of high wind speed data, impeding the preservation of relevant typhoon information for marine disaster monitoring. While in areas close to land, MLE is susceptible to land-induced noise, leading to the elimination of

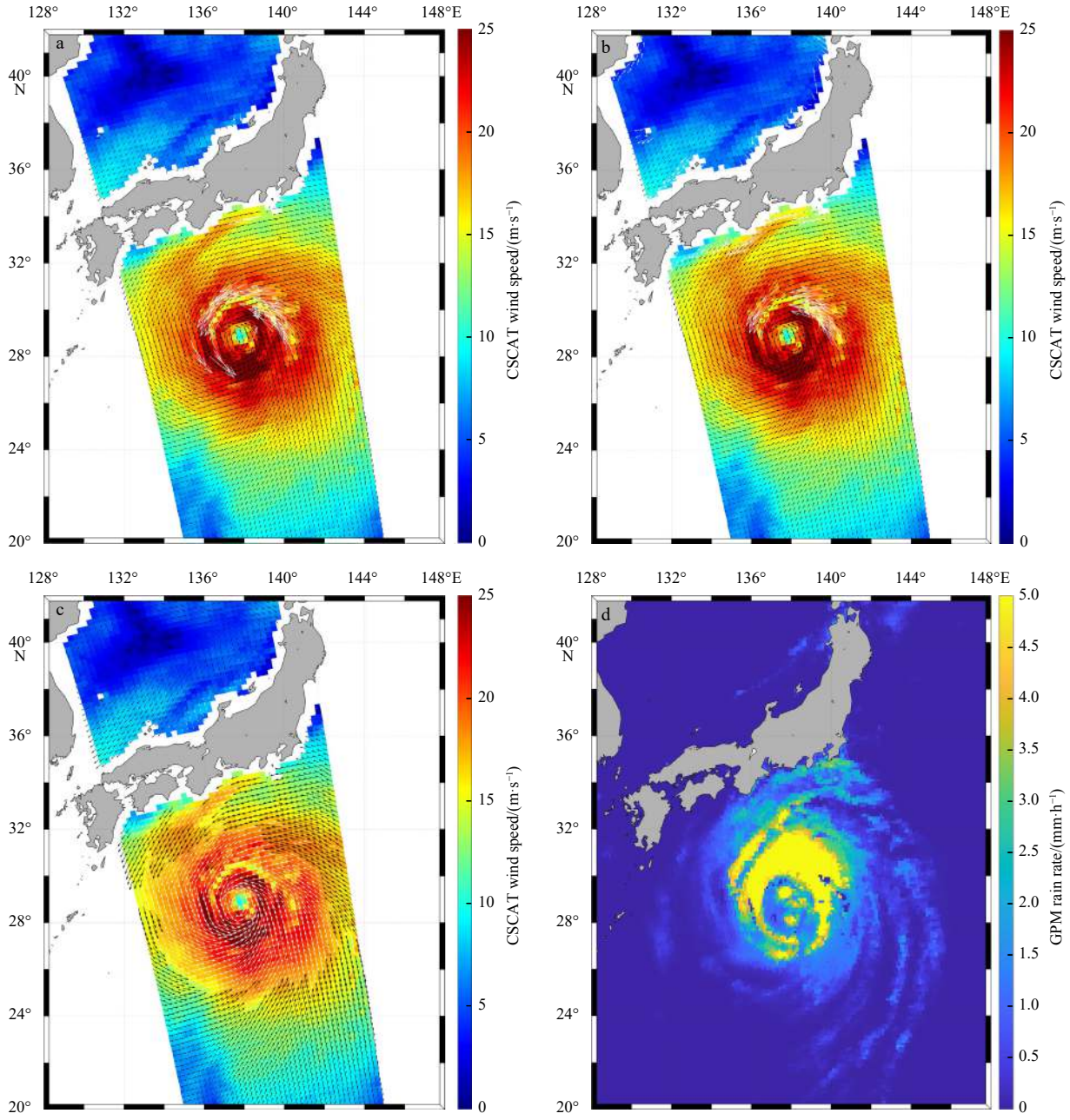

Fig. 5. CSCAT wind vectors superimposed on the map of wind speed (a–c) and the collocated GPM rain rate (d). White (black) arrows indicate the winds rejected (accepted) by the maximum likelihood estimator -based quality control (a), the averaged MLE-based quality control (b), and the singularity exponents-based quality control (c).

most coastal WVCs. In contrast, SE allows for the retention of more coastal WVCs. Therefore, one needs to examine carefully which quality indicators should be employed in practical applications in order to acquire the necessary wind data.

4.3 *Verification*

Following the above discussions, SE is more likely to identify low-quality WVCs in the nadir region and the outer swath, it is therefore chosen as the quality indicator for these two swath regions. In addition, compared to both MLE and SE, MLE_m tends to improve the wind QC at the sweet swath, such that it is selected as the optimal QC indicator for this region. Figure 6 illustrates the results, including correlation coefficient (CC), bias, standard deviation (SD), and VRMS, of the newly proposed QC method, i.e., the combination of SE and MLE_m, for CSCAT. For the sake of comparison, the single-indicator-based QC results are also shown in Fig. 6. It can be found that the MLE_m-based method rejects a smaller number of WVCs, but this brings a larger standard deviation of wind speed and direction, while the SE-based method retains a similar number of WVCs, and the data quality is improved to some extent. Therefore, the proposed method combines the features of MLE_m and SE, and demonstrates a reduction in wind speed bias while retaining a larger number of WVCs.

5 Conclusions

The primary objective of this study is to investigate suitable quality indicators for CSCAT, a Ku-band scatterometer with an innovative rotation fan-beam mechanism. The goal is to retain as many good-quality WVCs as possible, while discarding most of the low-quality ones. The study compares the QC results of MLE, MLE_m, and SE under various wind speed and WVC location conditions. The sensitivity of QC indicators to wind quality is mainly evaluated by comparing the VRMS differences between scatterometer and buoy winds. To mitigate the effect of data amount in the comparison, an identical rejection rate as a function of wind speed is applied to each quality indicator. SE has proved to be effective in discerning wind data quality over all wind speed bins and at the nadir region and the outer swath. Regarding the capability of different indicators for rain identification, it is found that MLE_m performs better than MLE and SE under medium wind speeds, while SE identifies the largest amount of rainy WVCs under low and high winds, probably due to that rain-in-

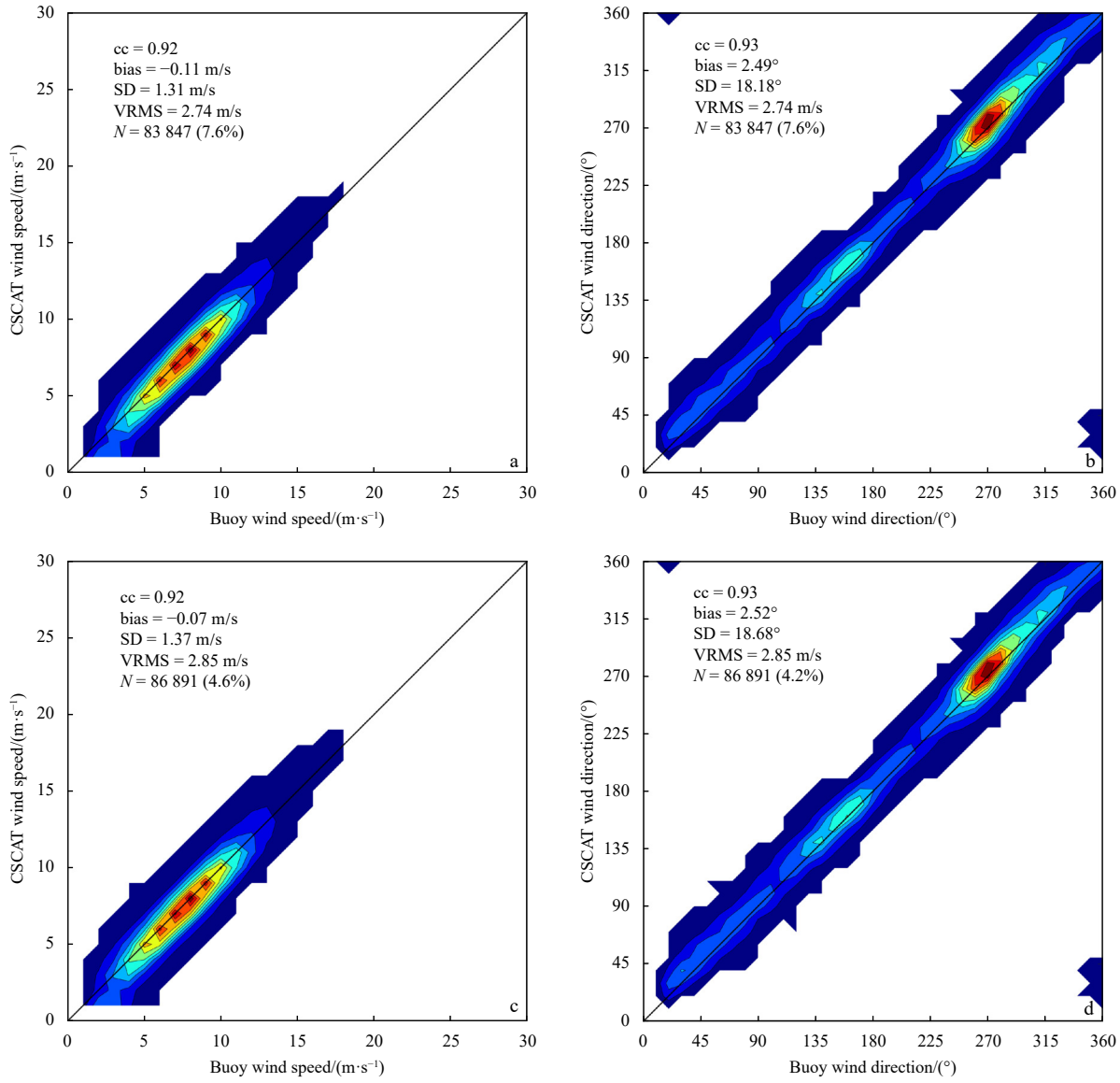

Fig. 6.

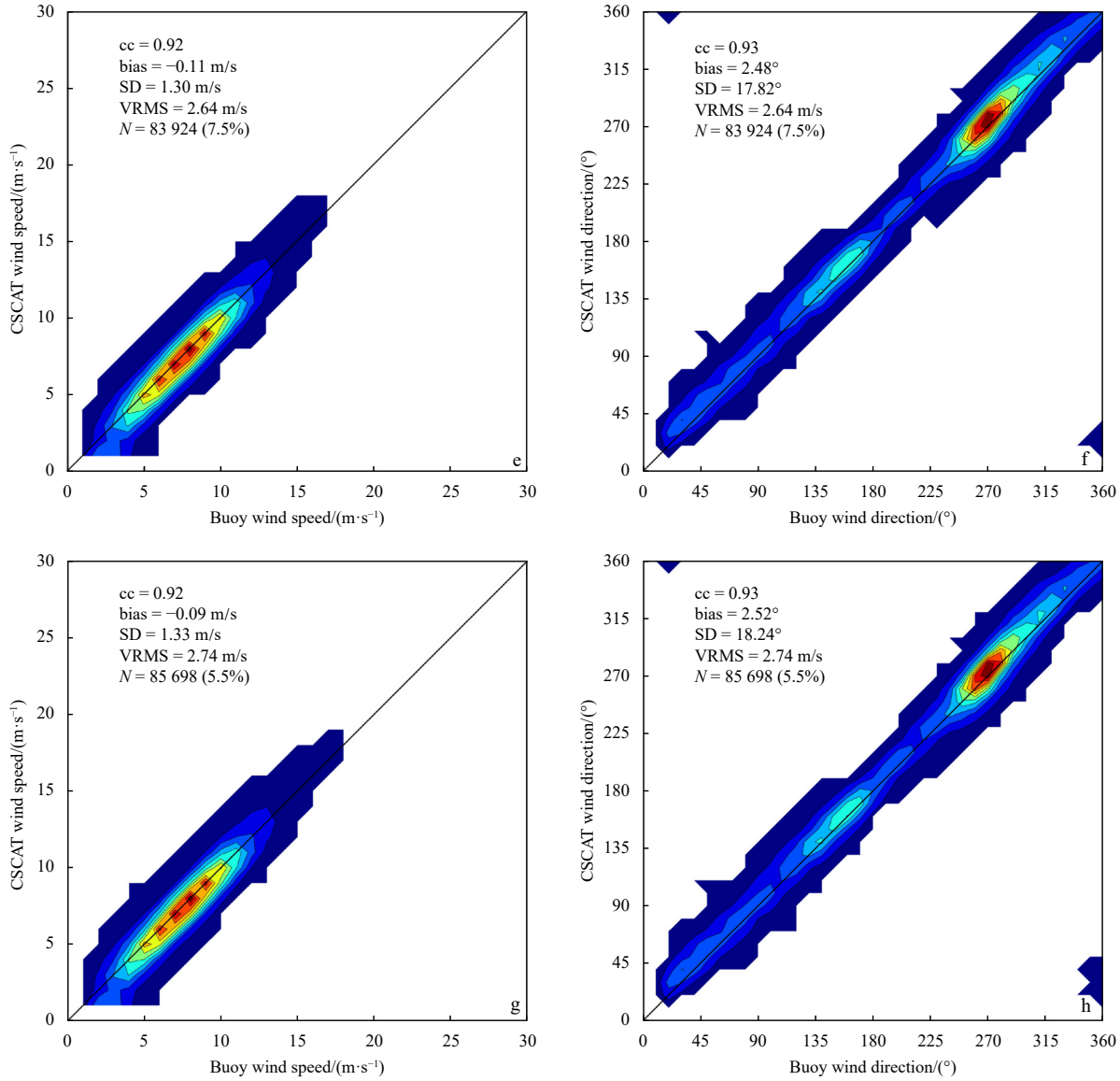

Fig. 6. China-France Oceanography Satellite scatterometer reprocessed winds versus buoy wind speed (a, c, e, and g) and wind direction(b, d, f, and h) accepted by the operational maximum likelihood estimator (MLE)-based quality control, averaged MLE-based quality control, SE-based quality control, and the proposed new quality control, respectively.

duced wind variability is most likely to associate with low and high winds. Notably, MLE_m shows the best sensitivity to rainfall regardless of the WVC location, possibly due to that most of the data are indeed collected at moderate wind speeds. Consequently, a QC method based on the combination of SE and MLE_m is proposed for CSCAT, that is SE is employed at the nadir region and outer swath, while MLE_m is utilized at the sweet region. The exploration of QC rejection rates for different CSCAT wind speeds will be done in our future research, aiming to further improve the quality of CSCAT winds.

Acknowledgements

The authors would like to acknowledge NSOAS for straightforward and rapid access to the CSCAT data and NASA for the GPM precipitation product.

References

Brennan M J, Hennon C C, Knabb R D. 2009. The operational use of QuikSCAT ocean surface vector winds at the National Hurricane Center. Weather and Forecasting, 24(3): 621–645, doi: 10.1175/2008WAF2222188.1

Chen Yaodeng, Cui Yemeng, Lin Wenming, et al. 2023. The impacts of assimilating CFOSAT scatterometer winds for Typhoon cases based on real-time rain quality control. Atmospheric Research, 285: 106621, doi: 10.1016/j.atmosres.2023.106621

Huddleston J N, Stiles B W. 2000. A multidimensional histogram rain-flagging technique for SeaWinds on QuikSCAT. In: Proceedings of the IGARSS 2000. IEEE 2000 International Geoscience and Remote Sensing Symposium. Honolulu, HI, USA: IEEE, 3: 1232–1234,doi: 10.1109/IGARSS.2000.858077

Huffman G J, Bolvin D T, Braithwaite D, et al. 2018. NASA global precipitation measurement (GPM) integrated multi-satellite retrievals for GPM (IMERG). Greenbelt, MD, USA: NASA. https://gpm.nasa.gov/sites/default/files/document_files/IMERG_ATBD_V5.2_0.pdf [2018-02-07/2023-12-20]

Lang Shuyan, Lin Wenming, Zhang Yi, et al. 2022. On the quality control of HY-2 scatterometer high winds. Remote Sensing, 14(21): 5565, doi: 10.3390/rs14215565

Lin Wenming, Dong Xiaolong, Portabella M, et al. 2019. A perspective on the performance of the CFOSAT rotating fan-beam scat-

terometer. IEEE Transactions on Geoscience and Remote Sensing, 57(2): 627–639, doi: 10.1109/TGRS.2018.2858852
Lin Wenming, Portabella M. 2017. Toward an improved wind quality control for RapidScat. IEEE Transactions on Geoscience and Remote Sensing, 55(7): 3922–3930, doi: 10.1109/TGRS.2017.2683720
Lin Wenming, Portabella M, Stoffelen A, et al. 2014. Rain identification in ASCAT winds using singularity analysis. IEEE Geoscience and Remote Sensing Letters, 11(9): 1519–1523, doi: 10.1109/LGRS.2014.2298095
Lin Wenming, Portabella M, Stoffelen A, et al. 2015a. ASCAT wind quality control near rain. IEEE Transactions on Geoscience and Remote Sensing, 53(8): 4165–4177, doi: 10.1109/TGRS.2015.2392372
Lin Wenming, Portabella M, Stoffelen A, et al. 2015b. ASCAT wind quality under high subcell wind variability conditions. Journal of Geophysical Research: Oceans, 120(8): 5804–5819, doi: 10.1002/2015JC010861
Lin Wenming, Portabella M, Turiel A, et al. 2016. An improved singularity analysis for ASCAT wind quality control: Application to low winds. IEEE Transactions on Geoscience and Remote Sensing, 54(7): 3890–3898, doi: 10.1109/TGRS.2016.2529700
Liu W T, Katsaros K B, Businger J A. 1979. Bulk parameterization of air-sea exchanges of heat and water vapor including the molecular constraints at the interface. Journal of the Atmospheric Sciences, 36(9): 1722–1735, doi: 10.1175/1520-0469(1979)036<1722:BPOASE>2.0.CO;2
Liu Jianqiang, Lin Wenming, Dong Xiaolong, et al. 2020. First results from the rotating fan beam scatterometer onboard CFOSAT. IEEE Transactions on Geoscience and Remote Sensing, 58(12): 8793–8806, doi: 10.1109/TGRS.2020.2990708
Liu Siqi, Lin Wenming, Portabella M, et al. 2022. Characterization of tropical cyclone intensity using the HY-2B scatterometer wind data. Remote Sensing, 14(4): 1035, doi: 10.3390/rs14041035
Mironov A S, Quilfen Y, Piolle J F, et al. 2023. A method for continues calibration of a rotating antenna scatterometer in application to CFOSAT measurements. In: Proceedings of the IGARSS 2023-2023 IEEE International Geoscience and Remote Sensing Symposium. Pasadena, CA, USA: IEEE, 4072–4075
Mou Xiaoheng, Lin Wenming, He Yijun. 2023. Towards a consistent wind data record for the CFOSAT scatterometer. Remote Sensing, 15(8): 2081, doi: 10.3390/rs15082081
Peng Yihuan, Xie Xuetong, Lin Mingsen, et al. 2021. A study of sea surface rain identification based on HY-2A scatterometer. Remote Sensing, 13(17): 3475, doi: 10.3390/rs13173475
Pierson Jr W J. 1989. Probabilities and statistics for backscatter estimates obtained by a scatterometer. Journal of Geophysical Research: Oceans, 94(C7): 9743–9759
Portabella M, Lin Wenming, Stoffelen A, et al. 2021. Consolidation of quality control procedures for scatterometers. In: Proceedings of the 2021 IEEE International Geoscience and Remote Sensing Symposium IGARSS. Brussels, Belgium: IEEE, 1630–1633
Portabella M, Stoffelen A. 2001. Rain detection and quality control of SeaWinds. Journal of Atmospheric and Oceanic Technology, 18(7): 1171–1183, doi: 10.1175/1520-0426(2001)018<1171:RDAQCO>2.0.CO;2
Portabella M, Stoffelen A. 2002a. A comparison of KNMI quality control and JPL rain flag for SeaWinds. Canadian Journal of Remote Sensing, 28(3): 424–430, doi: 10.5589/m02-040
Portabella M, Stoffelen A. 2002b. Characterization of residual information for SeaWinds quality control. IEEE transactions on geoscience and remote sensing, 40(12): 2747–2759, doi: 10.1109/TGRS.2002.807750
Portabella M, Stoffelen A, Lin Wenming, et al. 2012. Rain effects on ASCAT-retrieved winds: Toward an improved quality control. IEEE Transactions on Geoscience and Remote Sensing, 50(7): 2495–2506, doi: 10.1109/TGRS.2012.2185933
Prakash S, Mitra A K, Pai D S, et al. 2016. From TRMM to GPM: How well can heavy rainfall be detected from space?. Advances in Water Resources, 88: 1–7
Stiles B W, Dunbar R S. 2010. A neural network technique for improving the accuracy of scatterometer winds in rainy conditions. IEEE Transactions on Geoscience and Remote Sensing, 48(8): 3114–3122, doi: 10.1109/TGRS.2010.2049362
Stiles B W, Yueh S H. 2002. Impact of rain on spaceborne Ku-band wind scatterometer data. IEEE Transactions on Geoscience and Remote Sensing, 40(9): 1973–1983, doi: 10.1109/TGRS.2002.803846
Stoffelen A, Anderson D. 1997. Scatterometer data interpretation: Measurement space and inversion. Journal of Atmospheric and Oceanic Technology, 14(6): 1298–1313, doi: 10.1175/1520-0426(1997)014<1298:SDIMSA>2.0.CO;2
Stoffelen A, Portabella M. 2006. On Bayesian scatterometer wind inversion. IEEE Transactions on Geoscience and Remote Sensing, 44(6): 1523–1533, doi: 10.1109/TGRS.2005.862502
Tournadre J, Quilfen Y. 2003. Impact of rain cell on scatterometer data: 1. Theory and modeling. Journal of Geophysical Research: Oceans, 108(C7): 3225
Verhoef A, Vogelzang J, Verspeek J, et al. 2015. PenWP user manual and reference guide. KNMI, De Bilt, the Netherlands: NWP SAF Rep. NWPSAF-KN-UD-009. https://knmi-scatterometer-website-prd.s3.amazonaws.com/publications/NWPSAF-KN-UD-009_PenWP_User_Guide_v4.0.pdf [2022-08/2023-12-23]
Weissman D E, Bourassa M A. 2008. Measurements of the effect of rain-induced sea surface roughness on the QuikSCAT scatterometer radar cross section. IEEE Transactions on Geoscience and Remote Sensing, 46(10): 2882–2894, doi: 10.1109/TGRS.2008.2001032
Xu Ying, Liu Jianqiang, Xie Lingling, et al. 2019. China-France Oceanography Satellite (CFOSAT) simultaneously observes the typhoon-induced wind and wave fields. Acta Oceanologica Sinica, 38(11): 158–161, doi: 10.1007/s13131-019-1506-3
Xu Xingou, Stoffelen A. 2020. Improved rain screening for Ku-band wind scatterometry. IEEE Transactions on Geoscience and Remote sensing, 58(4): 2494–2503, doi: 10.1109/TGRS.2019.2951726
Xu Xingou, Stoffelen A, Lin Wenming, et al. 2022. Rain false-alarm-rate reduction for CSCAT. IEEE Geoscience and Remote Sensing Letters, 19: 1–5
Zhao Xiaokang, Lin Wenming, Portabella M, et al. 2022. Effects of rain on CFOSAT scatterometer measurements. Remote Sensing of Environment, 274: 113015, doi: 10.1016/j.rse.2022.113015